RESEARCH BRIEF

Distinct Tumor Necrosis Factor Alpha Receptors Dictate Stem Cell Fitness versus Lineage Output in *Dnmt3a*-Mutant Clonal Hematopoiesis

Jennifer M. SanMiguel[1], Elizabeth Eudy[1], Matthew A. Loberg[1], Kira A. Young[1], Jayna J. Mistry[1], Kristina D. Mujica[1], Logan S. Schwartz[1,2], Timothy M. Stearns[1], Grant A. Challen[3], and Jennifer J. Trowbridge[1,2]

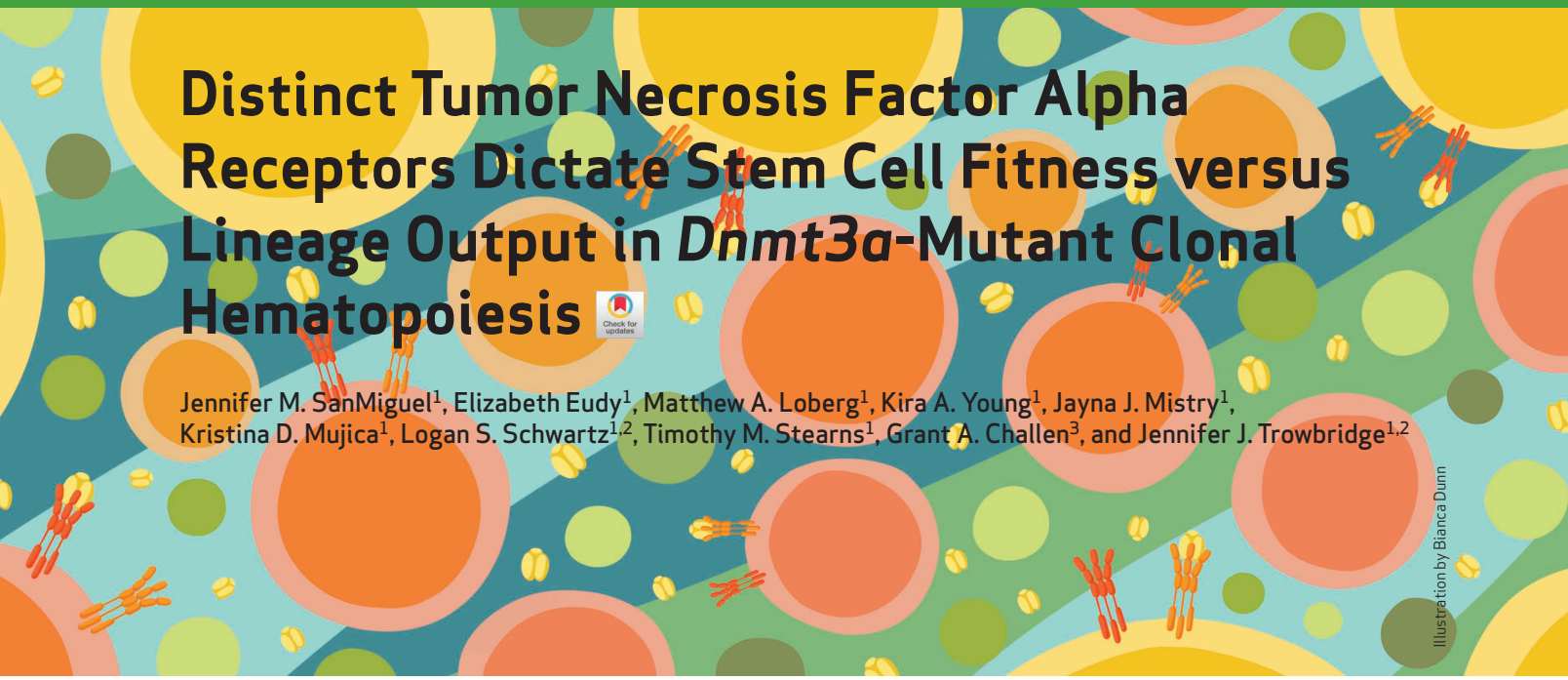

Illustration by Bianca Dunn

ABSTRACT Clonal hematopoiesis resulting from the enhanced fitness of mutant hematopoietic stem cells (HSC) associates with both favorable and unfavorable health outcomes related to the types of mature mutant blood cells produced, but how this lineage output is regulated is unclear. Using a mouse model of a clonal hematopoiesis–associated mutation, *DNMT3A*$^{R882/+}$ (*Dnmt3a*$^{R878H/+}$), we found that aging-induced TNFα signaling promoted the selective advantage of mutant HSCs and stimulated the production of mutant B lymphoid cells. The genetic loss of the TNFα receptor TNFR1 ablated the selective advantage of mutant HSCs without altering their lineage output, whereas the loss of TNFR2 resulted in the overproduction of mutant myeloid cells without altering HSC fitness. These results nominate TNFR1 as a target to reduce clonal hematopoiesis and the risk of associated diseases and support a model in which clone size and mature blood lineage production can be independently controlled to modulate favorable and unfavorable clonal hematopoiesis outcomes.

SIGNIFICANCE: Through the identification and dissection of TNFα signaling as a key driver of murine *Dnmt3a*-mutant hematopoiesis, we report the discovery that clone size and production of specific mature blood cell types can be independently regulated.

See related commentary by Niño and Pietras, p. 2724.

INTRODUCTION

Clonal hematopoiesis is an aging-associated condition in which hematopoietic stem cells (HSC) have acquired a somatic mutation or copy-number alteration that places them at a selective advantage. Both favorable and unfavorable health conditions have been associated with clonal hematopoiesis. Large clone size [variant allele frequency (VAF) >0.02] is associated with increased risk of hematologic malignancy, atherosclerosis, cardiovascular disease, type 2 diabetes, and osteoporosis (1–3). Many of these conditions have been related to abnormal production of proinflammatory myeloid cell types such as macrophages and mast cells (4). However, clonal hematopoiesis is naturally found in very aged populations without compromising survival (5) and is associated with a reduced risk of Alzheimer disease (6). Furthermore, clonal

[1]The Jackson Laboratory, Bar Harbor, Maine. [2]Graduate School of Biomedical Sciences, Tufts University, Boston, Massachusetts. [3]Division of Oncology, Department of Medicine, Washington University School of Medicine, St. Louis, Missouri.

Corresponding Author: Jennifer J. Trowbridge, The Jackson Laboratory, 600 Main Street, Bar Harbor, ME 04609. Phone: 207-288-6183; E-mail: jennifer.trowbridge@jax.org

Cancer Discov 2022;12:2763–73

doi: 10.1158/2159-8290.CD-22-0086

hematopoiesis driven by mutations in the DNA methyltransferase *DNMT3A* has been associated with increased survival of recipients after bone marrow (BM) transplantation related to mutant T lymphoid cell production (7) and maintenance of functional T-cell immunity in a supercentenarian (8). Thus, rather than developing methods to reduce clonal hematopoiesis altogether, further understanding of the molecular basis of both clone size and lineage output has the potential to empower strategies to harness beneficial aspects of clonal hematopoiesis as well as reduce adverse health risks. Here, we used a mouse model of a clonal hematopoiesis-associated mutation in *DNMT3A* (*Dnmt3a*$^{R878H/+}$; ref. 9) to study the molecular basis of HSC competition and lineage output.

RESULTS

Our group recently found that the middle-aged BM microenvironment drives HSC aging (10). This work established an experimental paradigm to evaluate the potency of *Dnmt3a*$^{R878H/+}$ HSCs in the aged BM microenvironment and identify HSC-extrinsic factors that modulate their selective advantage. We transplanted *Dnmt3a*$^{R878H/+}$ HSCs into young and middle-aged recipient mice (Fig. 1A). *Dnmt3a*$^{R878H/+}$ HSCs transplanted into aged recipients generated greater long-term multilineage hematopoiesis compared with control HSCs (Fig. 1B and C; Supplementary Fig. S1A) and gave rise to expanded HSC and multipotent progenitor (MPP) populations (Fig. 1D and E; Supplementary Fig. S1B). In addition, aged recipients had higher proportions of *Dnmt3a*$^{R878H/+}$ megakaryocyte and erythroid–primed MPPs (MPP$^{Mk/E}$) and lymphoid-primed MPPs (MPP^{Ly}; Fig. 1E). The latter was consistent with increased mature *Dnmt3a*$^{R878H/+}$ B lymphoid cells (Supplementary Fig. S1A). No change in the frequency of mature T lymphoid cells was observed, which may be explained in part by thymic involution during aging (11). Together, we find that *Dnmt3a*$^{R878H/+}$ HSCs have enhanced selective advantage over wild-type HSCs as well as altered lineage output in the context of the aged BM microenvironment.

To identify molecular signatures underlying expanded *Dnmt3a*$^{R878H/+}$ hematopoiesis in the aged BM microenvironment, we performed RNA sequencing (RNA-seq) on independent biological replicates of HSCs reisolated from young and aged recipient mice. Our experimental design specified only a sublethal dose of irradiation to recipient mice to better preserve HSC-extrinsic signals from the BM microenvironment (refs. 12, 13; Supplementary Fig. S1C). A greater number of differentially expressed genes in *Dnmt3a*$^{R878H/+}$ versus control HSCs were found in aged compared with young recipient mice (Fig. 1F). Gene and pathway enrichment analyses identified TNFα as the top enriched gene signature and predicted upstream regulator in *Dnmt3a*$^{R878H/+}$ HSCs in aged mice (Fig. 1G). Complementary to this, we found increased levels of TNFα in the BM fluid of aged compared with young mice, as well as mice transplanted with *Dnmt3a*$^{R878H/+}$ versus control hematopoietic cells (Supplementary Fig. S1D and S1E). This is consistent with a previous report that circulating TNFα is significantly increased in humans with *DNMT3A*-mutant clonal hematopoiesis, relative to other clonal hematopoiesis mutations (14). A previously described TNFα-induced transcriptional program in HSCs, enriched in prosurvival genes (15), was elicited in *Dnmt3a*$^{R878H/+}$ HSCs in aged mice (Supplementary Fig. S1F). In addition, *Dnmt3a*$^{R878H/+}$ HSCs in aged mice sustained expression of transcriptional programs that define mouse and human HSCs (refs. 16, 17; Supplementary Fig. S1D). In humans, *DNMT3A*$^{R882H/+}$ CD34$^+$ hematopoietic stem/progenitor cells (HSPC) were enriched for TNFα pathway genes compared with *DNMT3A*$^{+/+}$ CD34$^+$ HSPCs isolated from the same individuals (Fig. 1H; ref. 18). Several TNFα target genes were commonly upregulated in human *DNMT3A*$^{R882H/+}$ CD34$^+$ HSPCs and mouse *Dnmt3a*$^{R878H/+}$ HSCs, including *JUN* and *NFKB2* (Fig. 1I). Thus, the selective advantage of mouse and human *DNMT3A*-mutant HSCs positively correlates with elevated TNFα signaling.

To assess the extent to which TNFα directly promotes young *Dnmt3a*-mutant HSC survival, we added recombinant TNFα to mixed cultures of wild-type and *Dnmt3a*-mutant HSCs in media that sustain HSC self-renewal (ref. 19; Fig. 2A). TNFα treatment reduced the number of control but not *Dnmt3a*$^{R878H/+}$ cells produced over the culture period (Supplementary Fig. S2A). After culture, cells were transplanted into recipient mice to assess HSC function. TNFα-treated control HSCs did not sustain long-term multilineage engraftment (Fig. 2B; Supplementary Fig. S2B–S2E). In contrast, TNFα-treated *Dnmt3a*$^{R878H/+}$ HSCs increased the production of mature hematopoietic cells in the short term (4 weeks after transplant) followed by sustained multilineage engraftment. In addition, TNFα stimulation transiently increased *Dnmt3a*$^{R878H/+}$ B lymphoid cell production (Fig. 2C and D; Supplementary Fig. S2B) in contrast to myeloid regeneration from TNFα-treated control HSCs, as has been previously reported (15). In the BM, we observed trends toward reduced HSC, MPP$^{Mk/E}$, and granulocyte-macrophage–primed MPP (MPP$^{G/M}$) populations from TNFα-treated control HSCs, which was not observed in TNFα-treated *Dnmt3a*$^{R878H/+}$ HSCs (Supplementary Fig. S2F and S2G). Thus, TNFα-driven myeloid regeneration at the expense of HSC

Figure. 1. *Dnmt3a*$^{R878H/+}$ HSCs engage a TNFα-induced program in the aged BM microenvironment that is conserved in human *DNMT3A*-mutant clonal hematopoiesis. **A,** Schematic of the experimental design to compare Mx-Cre control and *Dnmt3a*$^{R878H/+}$ (R878H/+) engraftment in young (2–4 months) and aged (13–15 months) recipient mice. **B,** Frequency of donor (CD45.2$^+$) cells in the peripheral blood (PB) of recipient mice after transplant. Significance was calculated using two-way ANOVA with the Tukey multiple comparisons test. **C,** Frequency of donor cells in the BM of recipient mice. Significance was calculated using one-way ANOVA with the Bonferroni multiple comparisons test. **D,** Frequency of HSCs and MPPs in donor-derived BM cells. Significance was calculated using two-way ANOVA with Fisher's least significant difference (LSD) test. **E,** Frequency of MPP$^{Mk/E}$, MPP$^{G/M}$, and MPP^{Ly} in donor-derived BM cells. Significance was calculated using two-way ANOVA with Fisher's LSD test. **F,** Volcano plots with significantly differentially expressed genes (FDR <0.5, logFC >2) within colored boxes ($n = 2$–4 biological replicates). **G,** Enrichment of hallmark gene sets (left) and predicted upstream regulators (right) in control versus *Dnmt3a*$^{R878H/+}$ HSCs in aged recipient mice. IPA, Ingenuity Pathway Analysis. **H,** Hallmark TNF pathway enrichment across stem and progenitor populations between human *DNMT3A*^{R882H} versus control CD34$^+$ cells. EP, erythroid progenitor; IMP, immature myeloid progenitor; IMP-GM, granulo-monocytic–biased immature myeloid progenitor; IMP-ME, megakaryocytic-erythroid–biased immature myeloid progenitor; LMPP, lympho-myeloid–primed progenitor; MEP, megakaryocytic-erythroid progenitor; NP, neutrophil progenitor; PREB, pre-B cell progenitor. **I,** Overlap of differentially expressed genes in *DNMT3A*^{R882H} versus control CD34$^+$ cells and R878H/+ versus aged mouse HSCs. **B–E,** Dots represent individual recipient mice; boxes show 25th to 75th percentiles; line is median; and whiskers show min to max. *, $P < 0.05$; **, $P < 0.01$; ***, $P < 0.001$.

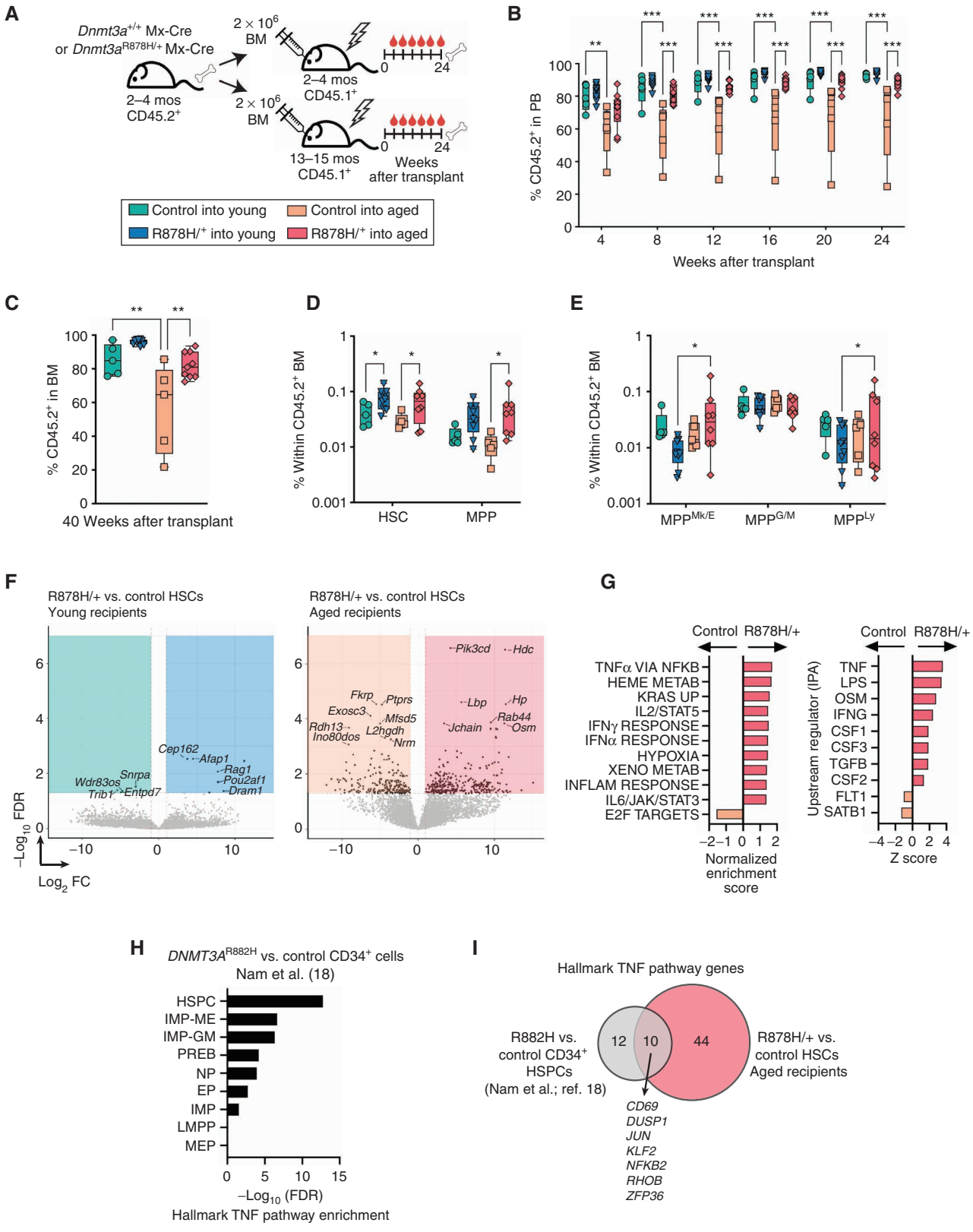
A
Dnmt3a+/+ Mx-Cre
or Dnmt3aR878H/+ Mx-Cre
2–4 mos
CD45.2+
2 × 10^6 BM
2–4 mos
CD45.1+
2 × 10^6 BM
13–15 mos
CD45.1+
0
24
Weeks after transplant
Control into young
Control into aged
R878H/+ into young
R878H/+ into aged
B
% CD45.2+ in PB
Weeks after transplant
C
% CD45.2+ in BM
40 Weeks after transplant
D
% Within CD45.2+ BM
HSC
MPP
E
% Within CD45.2+ BM
MPPMk/E
MPPG/M
MPPLy
F
R878H/+ vs. control HSCs
Young recipients
R878H/+ vs. control HSCs
Aged recipients
Cep162
Afap1
Rag1
Pou2af1
Dram1
Snrpa
Wdr83os
Trib1
Entpd7
Pik3cd
Hdc
Fkrp
Ptprs
Exosc3
Mfsd5
Rdh13
L2hgdh
Ino80dos
Nrm
Lbp
Hp
Jchain
Rab44
Osm
–Log10 FDR
Log2 FC
G
Control
R878H/+
TNFα VIA NFKB
HEME METAB
KRAS UP
IL2/STAT5
IFNγ RESPONSE
IFNα RESPONSE
HYPOXIA
XENO METAB
INFLAM RESPONSE
IL6/JAK/STAT3
E2F TARGETS
Normalized enrichment score
Upstream regulator (IPA)
TNF
LPS
OSM
IFNG
CSF1
CSF3
TGFB
CSF2
FLT1
SATB1
Z score
H
DNMT3AR882H vs. control CD34+ cells
Nam et al. (18)
HSPC
IMP-ME
IMP-GM
PREB
NP
EP
IMP
LMPP
MEP
–Log10 (FDR)
Hallmark TNF pathway enrichment
I
Hallmark TNF pathway genes
R882H vs. control CD34+ HSPCs (Nam et al.; ref. 18)
12
10
44
R878H/+ vs. control HSCs Aged recipients
CD69
DUSP1
JUN
KLF2
NFKB2
RHOB
ZFP36

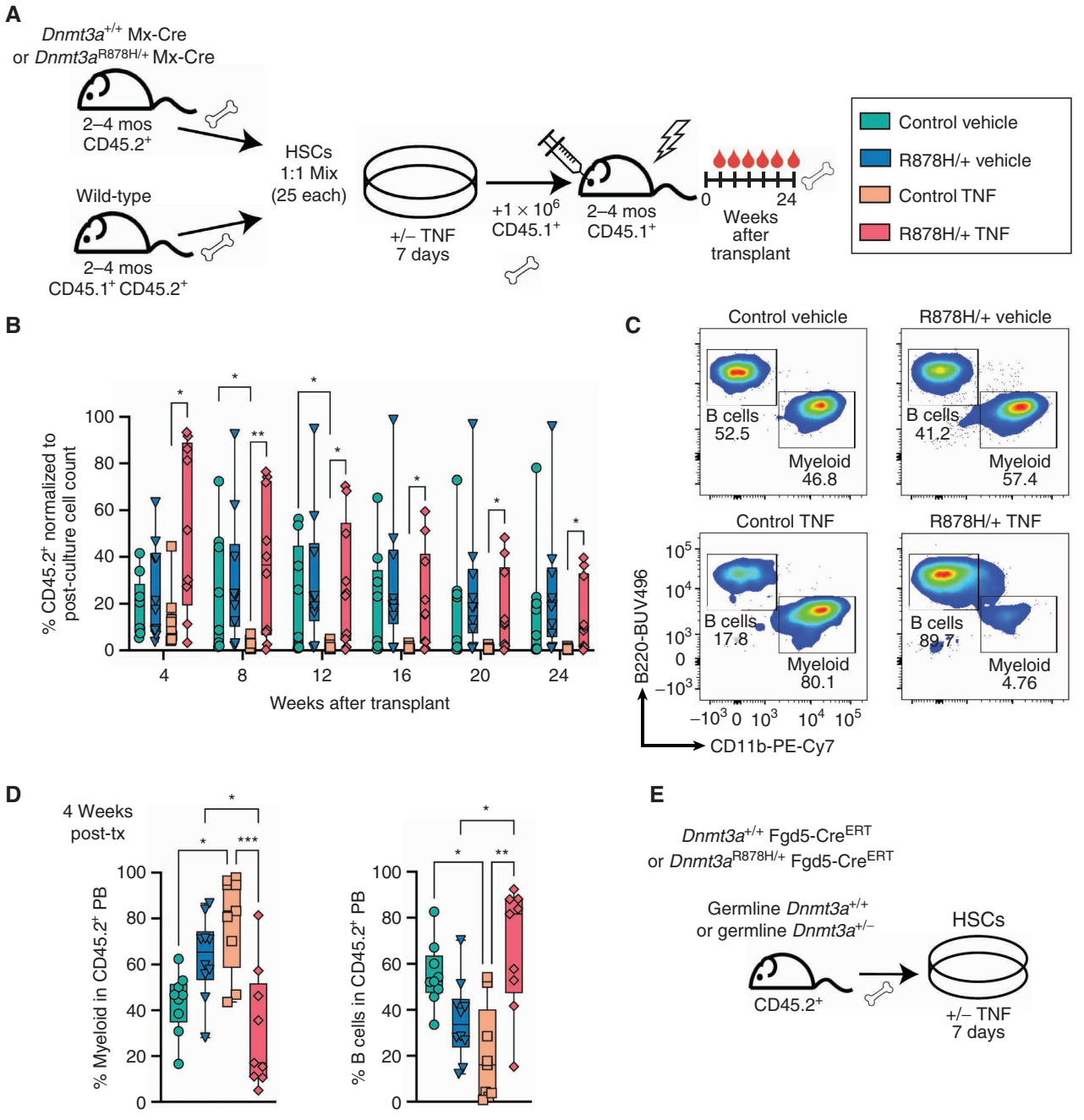

Figure 2. *Dnmt3a*-mutant HSCs maintain self-renewal and generate B lymphoid cells following TNF stimulation. **A,** Schematic of experimental design to test the response of Mx-Cre control and *Dnmt3a*$^{R878H/+}$ HSCs to recombinant TNFα *ex vivo* under growth conditions that favor HSC expansion. **B,** Normalized frequency of donor-derived cells in the peripheral blood (PB) of recipient mice after transplant. Significance was calculated using a mixed-effects model with Fisher's least significant difference (LSD) test. **C,** Representative flow cytometry plots showing B-cell and myeloid cell frequencies in donor-derived PB at 4 weeks after transplant. **D,** Frequency of myeloid (left) and B (right) cells in donor-derived PB at 4 weeks after transplant. Significance was calculated using two-way ANOVA with the Sidak multiple comparisons test. Post-tx, posttreatment. **E,** Schematic of experimental design to test TNFα response of *Fgd5*-Cre^{ERT} control versus *Fgd5*-Cre^{ERT} *Dnmt3a*$^{R878H/+}$ HSCs and germline *Dnmt3a*$^{+/+}$ verus *Dnmt3a*$^{+/-}$ HSCs. (*continued on following page*)

self-renewal is disrupted in *Dnmt3a*$^{R878H/+}$ HSCs. Instead, TNFα-treated *Dnmt3a*$^{R878H/+}$ HSCs favor lymphoid regeneration and maintain their self-renewal. To assess this in complementary models, we used tamoxifen-inducible *Fgd5*-Cre–driven *Dnmt3a*$^{R878H/+}$ mice as well as germline *Dnmt3a*$^{+/-}$ mice to isolate HSCs for TNFα stimulation (Fig. 2E). TNFα treatment reduced the number of control but not *Fgd5*-Cre *Dnmt3a*$^{R878H/+}$ cells (Fig. 2F) or *Dnmt3a*$^{+/-}$ cells (Fig. 2G) over the culture period. Upon transplant, TNFα-treated *Dnmt3a*$^{+/-}$ HSCs sustained multilineage engraftment at a higher frequency than TNFα-treated control HSCs (Fig. 2H). In addition, TNFα stimulation transiently increased *Dnmt3a*$^{+/-}$ B lymphoid relative to myeloid cell production (Fig. 2I; Supplementary Fig. S2H). Thus, TNFα-induced HSC survival

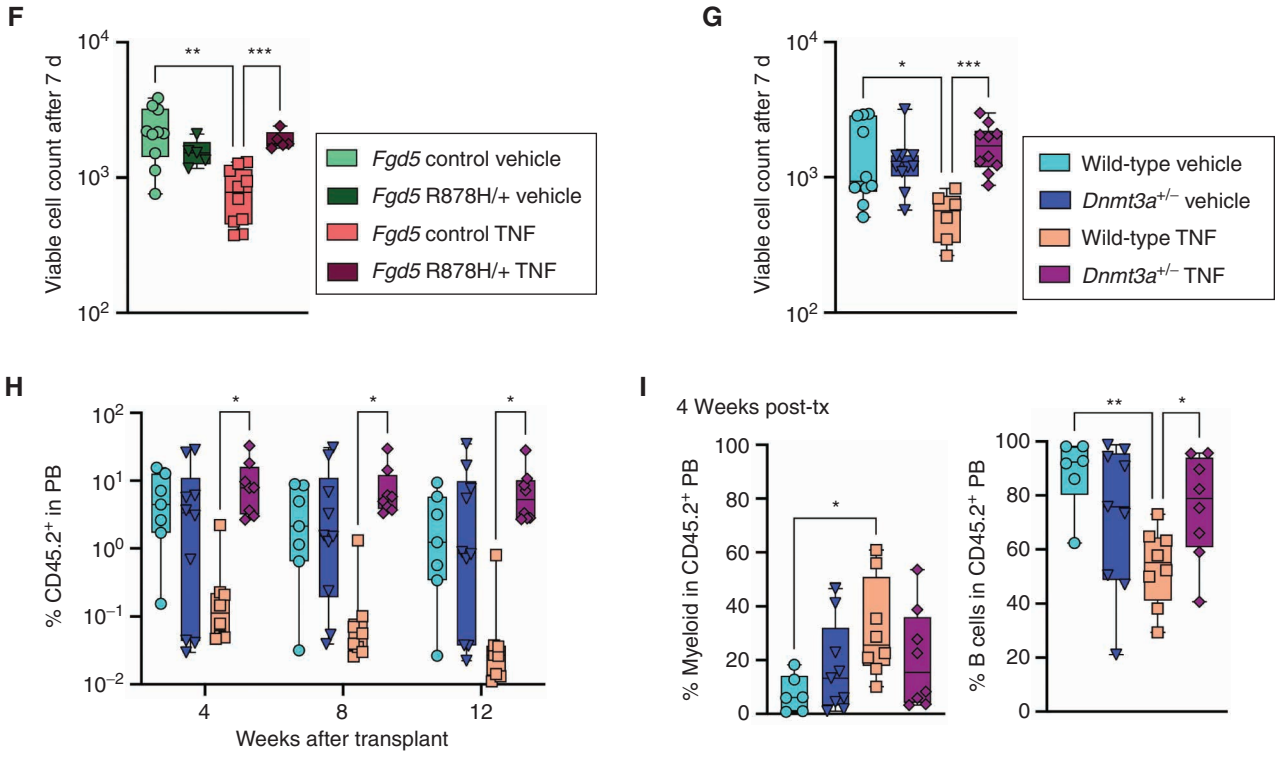

Figure 2. ***(Continued)*** **F** and **G,** Viable cell counts after 7 days of culture. Significance was calculated using Brown-Forsythe and Welch ANOVA with Welch correction. **H,** Frequency of donor-derived cells in PB of recipient mice after transplant. Significance was calculated using a mixed-effects model with Fisher's LSD test. **I,** Frequency of myeloid (left) and B (right) cells in donor-derived PB at 4 weeks after transplant. Significance was calculated using one-way ANOVA with Fisher's LSD test. **B, D,** and **F–I,** Dots represent individual recipient mice; boxes show 25th to 75th percentiles; line is median; and whiskers show min to max. *, $P < 0.05$; **, $P < 0.01$; ***, $P < 0.001$.

and disrupted myeloid regeneration are broadly relevant to *Dnmt3a*-mutant clonal hematopoiesis.

TNFα signaling occurs through two distinct TNFα receptors: TNFR1 (*Tnfrsf1a*) and TNFR2 (*Tnfrsf1b*). Both TNFR1 and TNFR2 are expressed on HSC and MPP populations and are not altered in surface expression between control and *Dnmt3a*$^{R878H/+}$ mice (Supplementary Fig. S3A–S3D). To determine which of these receptors are responsible for TNFα-mediated selective advantage of *Dnmt3a*$^{R878H/+}$ HSCs and B lymphoid cell production, we crossed *Dnmt3a*$^{R878H/+}$ mice with *Tnfrsf1a* or *Tnfrsf1b* knockout mice (Supplementary Fig. S3E) and tested HSC function by competitive serial BM transplantation into aged recipients (Fig. 3A; Supplementary Fig. S4A–S4F; Supplementary Fig. S5A–S5F). Loss of TNFR1, but not TNFR2, eliminated the selective advantage of *Dnmt3a*$^{R878H/+}$ peripheral blood (PB) and BM cells in secondary transplant recipients (Fig. 3B; Supplementary Fig. S5A). No change in engraftment was observed in TNFR1 knockout–only controls (Supplementary Fig. S6A–S6F; Supplementary Fig. S7A–S7G), demonstrating that this is a specific dependency of *Dnmt3a*$^{R878H/+}$ cells. In contrast, loss of TNFR2, but not TNFR1, reduced the proportion of B and T lymphoid cells and increased the proportion of myeloid cells (Fig. 3C and D) without altering overall white blood cell production (Supplementary Fig. S5B). Myeloid-biased hematopoiesis was also observed in TNFR2 knockout–only controls but only late in the post–secondary-transplant period (Supplementary Fig. S7C), and it did not increase neutrophil count (Supplementary Fig. S7B). Thus, distinct TNFα receptors mediate *Dnmt3a*$^{R878H/+}$ HSC regenerative capacity versus lineage output. We compared our TNFR knockout phenotypes with pharmacologic pan-TNFα blockade using etanercept (Fig. 3E). Etanercept reduced the competitive PB advantage of *Dnmt3a*$^{R878H/+}$ cells (Fig. 3F), trended toward reduction in BM engraftment (Fig. 3G), and reduced the frequency of *Dnmt3a*$^{R878H/+}$ HSC, MPP$^{Mk/E}$, and MPP^{Ly} populations (Fig. 3H). In contrast, etanercept produced a trend toward an increase of *Dnmt3a*$^{R878H/+}$ myeloid-primed MPP$^{G/M}$. Thus, pan-TNF inhibition results in a mix of our observed TNFR knockout phenotypes—that is, reduced selective advantage of *Dnmt3a*$^{R878H/+}$ hematopoiesis as well as myeloid lineage bias at the stem/progenitor cell level.

To interrogate the mechanisms by which TNFα signaling through different receptors affects *Dnmt3a*$^{R878H/+}$ cells, we harvested donor-derived HSPCs from secondary transplant recipient mice for single-cell RNA-seq ($n = 3$–4 biological replicates per genotype; Fig. 4A). After quality control filtering (Supplementary Fig. S8A–S8C), a total of 64,830 cells clustered into 22 populations (Fig. 4B). These clusters were classified based on published data to identify HSC, MPP, and lineage-specified progenitor subsets (ref. 20; Supplementary Fig. S8D and S8E; Supplementary Table S1). All clusters included cells expressing similar levels of *Tnfrsf1a* as well as *Tnfrsf1b* (Supplementary Fig. S8F). Pseudotime trajectory analysis revealed that myeloid

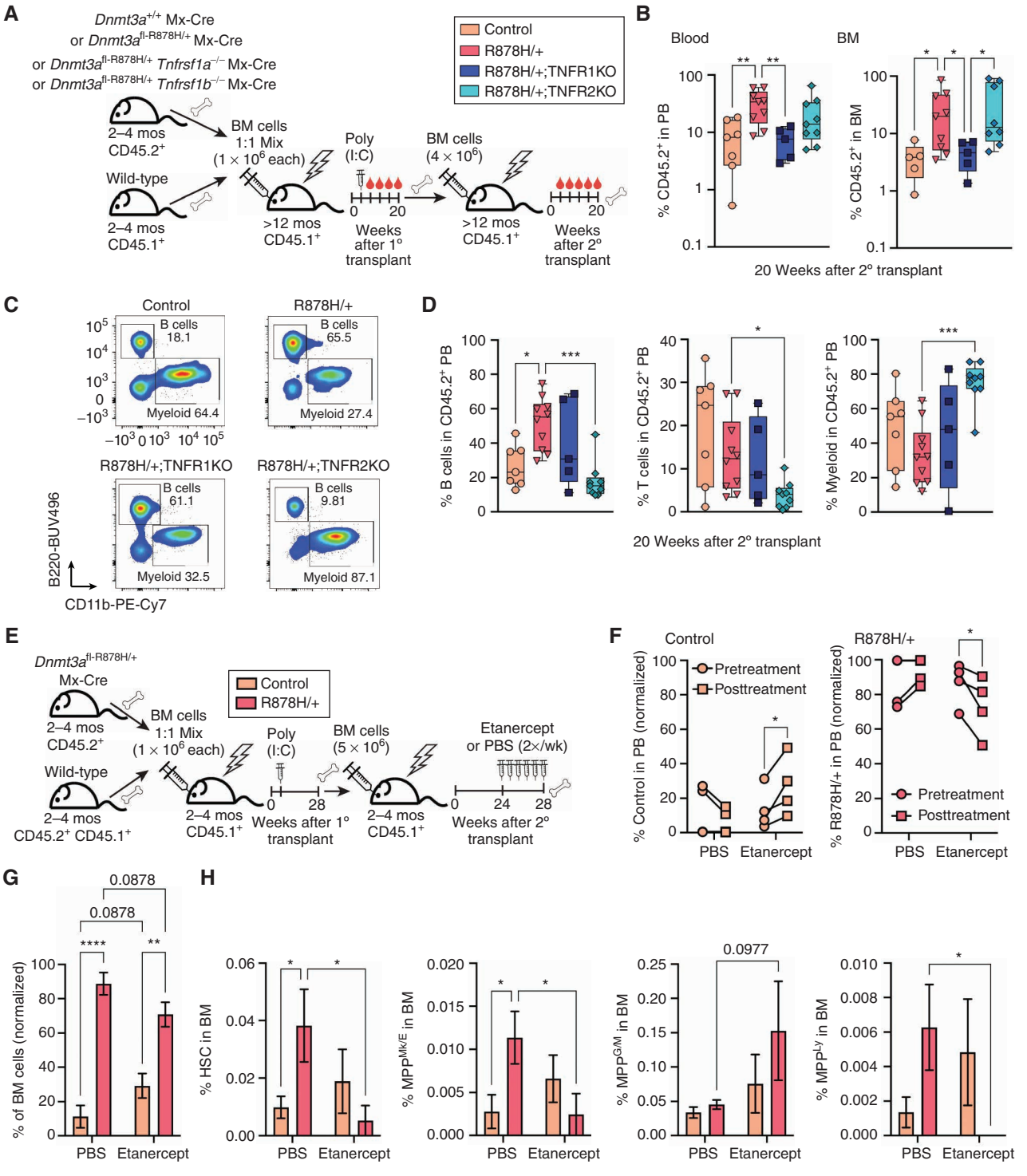

Figure 3. TNFR1 is required for *Dnmt3a*$^{R878H/+}$ HSC self-renewal, while TNFR2 regulates lymphoid cell production. **A,** Schematic of experimental design to test competitive, serial transplant of Mx-Cre control, *Dnmt3a*$^{R878H/+}$ (R878H/+), *Dnmt3a*$^{R878H/+}$ *Tnfrsf1a*$^{-/-}$ (R878H/+;TNFR1KO), and *Dnmt3a*$^{R878H/+}$ *Tnfrsf1b*$^{-/-}$ (R878H/+;TNFR2KO) in aged (>12 months) recipient mice. **B,** Frequency of donor cells in PB (left) and BM (right) of recipient mice at 20 weeks after secondary transplant. Significance was calculated using Brown-Forsythe and Welch ANOVA with Welch correction. **C,** Representative flow cytometry plots showing B-cell and myeloid cell frequencies in donor-derived PB. **D,** Frequency of B cells (left), T cells (center), and myeloid cells (right) in donor-derived PB at 20 weeks after secondary transplant. Significance was calculated using one-way ANOVA with the Tukey multiple comparisons test. **E,** Experimental schematic of transplant experiment with etanercept treatment. **F,** Frequency of control or R878H/+ donor cells in PB pre-and post-etanercept treatment. Significance was calculated using two-way ANOVA with Fisher's least significant difference (LSD) test. **G,** Frequency of control or R878H/+ donor cells in BM post-etanercept or vehicle treatment. Significance was calculated using two-way ANOVA with Fisher's LSD test. **H,** Frequency of HSC, MPP$^{Mk/E}$, MPP$^{G/M}$, and MPP^{Ly} populations in control or R878H/+ BM. Significance was calculated using two-way ANOVA with Fisher's LSD test. **B** and **D,** Dots represent individual recipient mice, boxes show 25th to 75th percentiles; line is median; and whiskers show min to max. **F,** Dots represent mean across biological replicates ($n = 4$). **G** and **H,** Bars represent mean ± SEM ($n = 4$). *, $P < 0.05$; **, $P < 0.01$; ***, $P < 0.001$; ****, $P < 0.0001$.

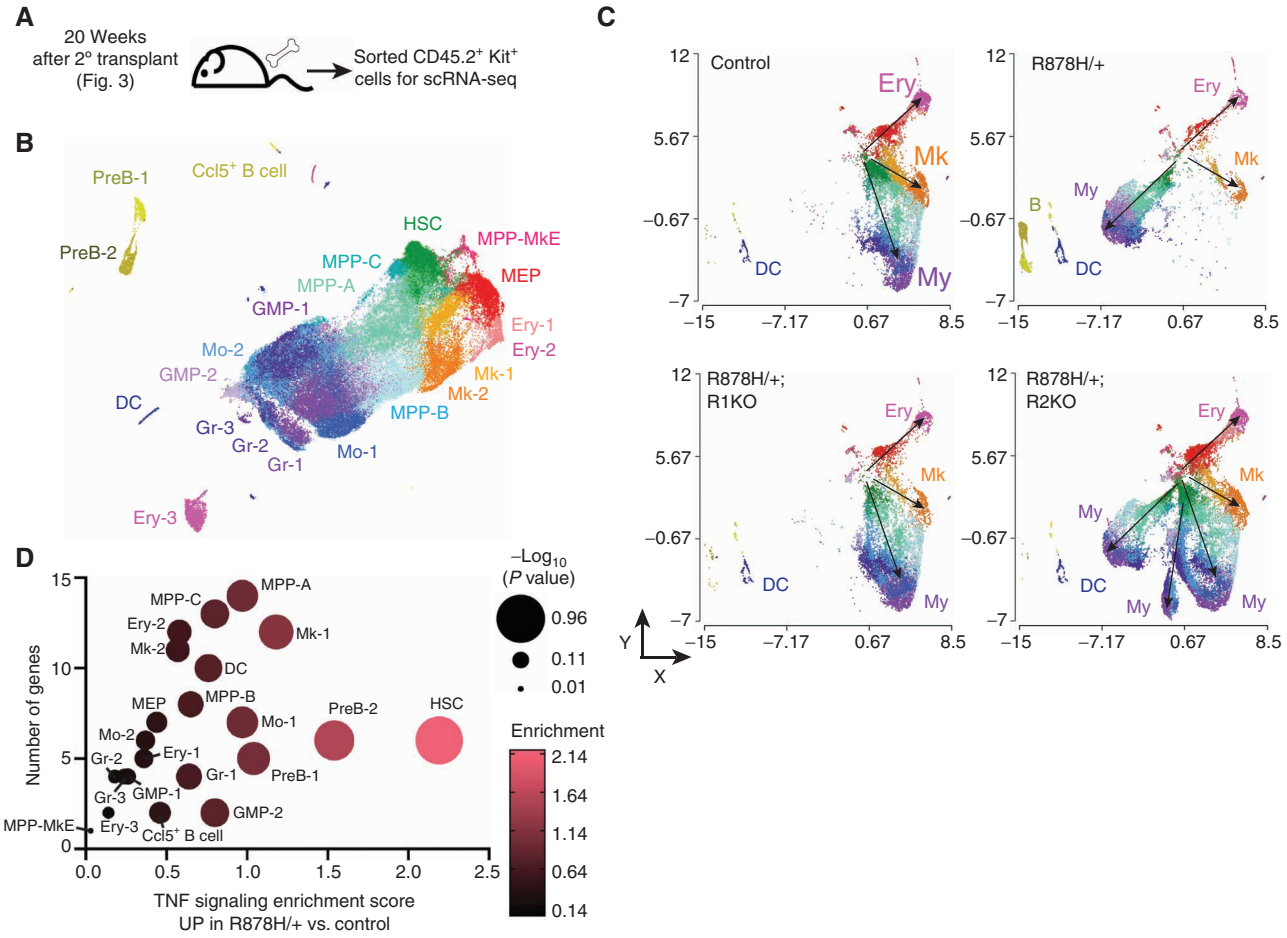

Figure 4. TNFR1 and TNFR2 engage distinct transcriptional programs in *Dnmt3a*$^{R878H/+}$ HSCs. **A,** Experimental schematic for single-cell RNA-seq (scRNA-seq). Data were collected from independent biological replicates of Mx-Cre control ($n = 3$), *Dnmt3a*$^{R878H/+}$ ($n = 4$), *Dnmt3a*$^{R878H/+}$ *Tnfrsf1a*$^{-/-}$ ($n = 3$), and *Dnmt3a*$^{R878H/+}$ *Tnfrsf1b*$^{-/-}$ ($n = 4$). **B,** Uniform Manifold Approximation and Projection (UMAP) of combined data identifying 22 cell clusters. DC, dendritic cell; Ery, erythroid; GMP, granulocyte-macrophage progenitor; Gr, granulocyte; MEP, megakaryocytic-erythroid progenitor; Mk, megakaryocyte; Mo, monocyte; My, myeloid; PreB, pre–B cell. **C,** Pseudotime visualization showing predicted differentiation trajectories from HSCs to erythroid, megakaryocyte, myeloid, B-cell (B), and dendritic cell lineages in each genotype pool. **D,** TNF signaling enrichment score in R878H/+ versus control cell clusters. (*continued on next page*)

progenitor differentiation from HSCs followed a distinct path in *Dnmt3a*$^{R878H/+}$ versus control BM (Fig. 4C), whereas erythroid and megakaryocyte progenitor differentiation paths were similar. Loss of TNFR1 fully corrected the aberrant *Dnmt3a*$^{R878H/+}$ HSC to myeloid progenitor differentiation trajectory to closely resemble control BM, whereas loss of TNFR2 created multiple myeloid differentiation trajectories from *Dnmt3a*$^{R878H/+}$ HSCs. These data are highly consistent with our functional observations that loss of TNFR1 eliminates *Dnmt3a*$^{R878H/+}$ selective advantage and loss of TNFR2 biases toward myeloid cell production. Within subsets of HSPCs, TNF signaling was most enriched in *Dnmt3a*$^{R878H/+}$ versus control HSCs (Fig. 4D), supporting that TNF-induced phenotypes are initiated at the HSC level. Indeed, many downstream TNF targets were increased in expression in *Dnmt3a*$^{R878H/+}$ versus control HSCs, and several of these target genes are known to be hypomethylated in *Dnmt3a*$^{R878H/+}$ HSCs (ref. 21; Fig. 4E). Examining the proportion of single HSCs that express *Tnfrsf1a* and/or *Tnfrsf1b* transcripts, we found that the majority (~70%) of HSCs had detectable *Tnfrsf1a* transcript only, ~15% of HSCs had detectable *Tnfrsf1b* transcript only, and the remaining ~15% of HSCs had both *Tnfrsf1a* and *Tnfrsf1b* transcripts (Supplementary Fig. S8G). This was modestly altered in *Dnmt3a*$^{R878H/+}$ HSCs with a trend toward more single *Tnfrsf1a*-expressing HSCs. Knockout of the opposing receptor did not transcriptionally alter receptor expression (Supplementary Fig. S8H). Focusing on unique transcriptional changes in *Dnmt3a*$^{R878H/+}$ TNFR1 versus TNFR2 knockout HSCs, we found that loss of TNFR1 resulted in increased expression of mediators of apoptosis, initiation factors for DNA repair and checkpoint activation, increased expression of *Cebpb*, and decreased cell division (Fig. 4E and F; Supplementary Fig. S8I). In contrast, loss of TNFR2 resulted in increased expression of the apoptosis inhibitor *Birc2*, a decrease in tumor suppressor p53, dysregulation of chromatin organization, and decreased B and T lymphoid "adaptive immune" signatures. Thus, TNFα–TNFR1 signaling promotes *Dnmt3a*$^{R878H/+}$ HSC competitive advantage through evasion of apoptosis, accumulation of

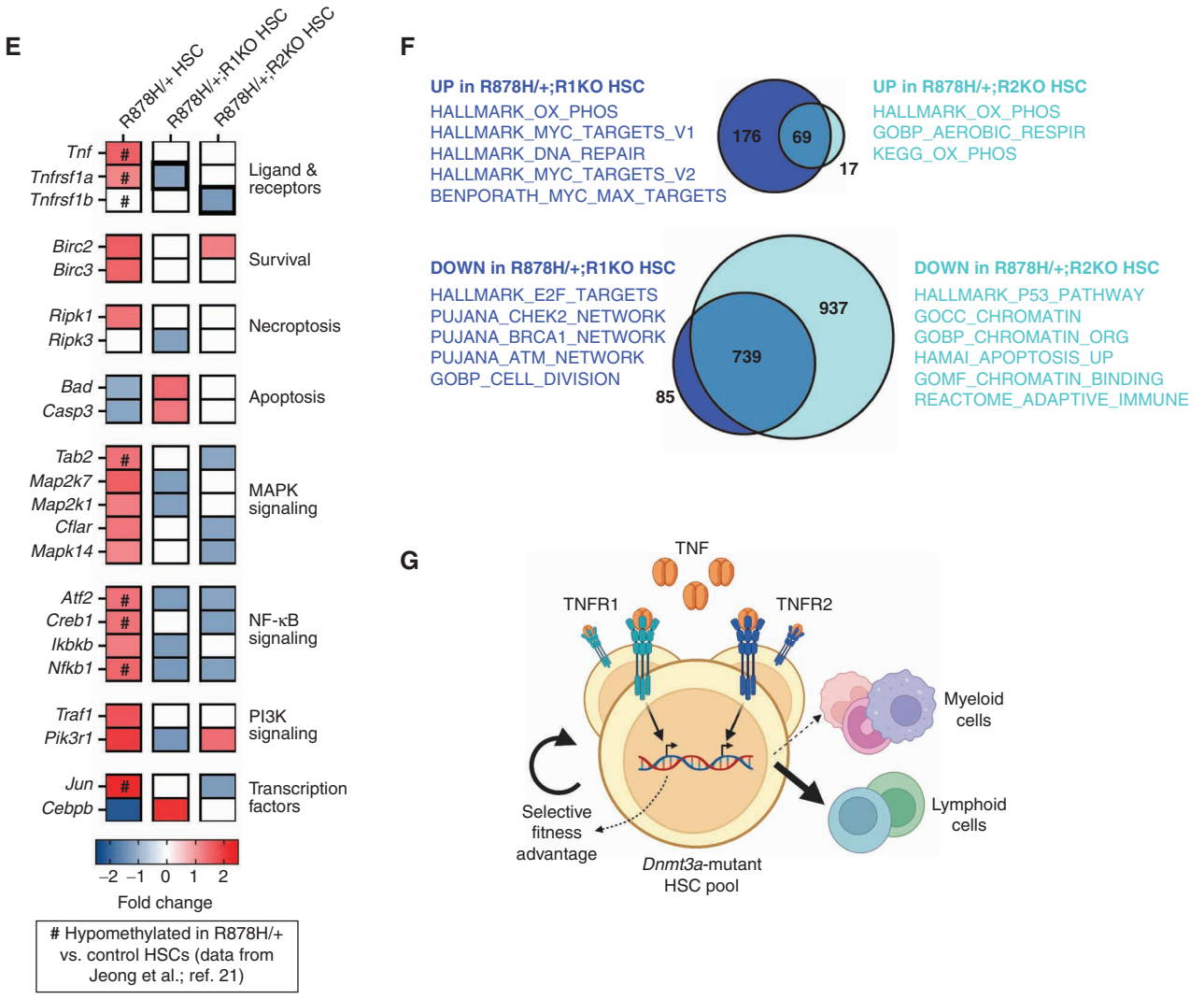

Figure 4. ***(Continued)*** **E,** Heat map representing fold change in expression of *Tnf*, *Tnfrsf1a* (TNFR1), *Tnfrsf1b* (TNFR2), and downstream TNF-regulated genes comparing R878H/+ versus control HSCs, R878H/+;R1KO versus R878H/+ HSCs, and R878H/+;R2KO versus R878H/+ HSCs. **#**, Loci hypomethylated in R878H/+ versus control HSCs (21). **F,** Venn diagrams of overlap between upregulated genes (top) and downregulated genes (bottom) in R878H/+;R1KO and R878H/+;R2KO HSCs compared with R878H/+ HSCs. From each comparison, unique gene lists were used to determine gene signature enrichment. **G,** Working model. TNFα–TNFR1 signaling dictates *Dnmt3a*-mutant HSC self-renewal, whereas TNFα–TNFR2 signaling promotes lymphoid lineage cell production. Decline in TNFα–TNFR2 signaling results in unrestrained production of *Dnmt3a*-mutant myeloid cells. (Created with BioRender.com, licensed by The Jackson Laboratory.)

DNA damage, self-renewal, and cell cycling. In contrast, TNFα–TNFR2 signaling promotes lymphoid cell production from *Dnmt3a*$^{R878H/+}$ HSCs, and restrains myeloid cell production, through chromatin regulation and expression of lymphoid-specifying genes.

DISCUSSION

Inhibition of proinflammatory cytokines, including TNFα, has been proposed as a generalizable strategy to reduce fitness of clonal hematopoiesis–mutant HSCs and risk of clonal hematopoiesis–associated disease states that are related to abnormal production of proinflammatory myeloid cells (22–26). Our work suggests that although pan-TNF inhibition does reduce *Dnmt3a*$^{R878H/+}$ HSC fitness, it also results in more complex and potentially detrimental effects due to unrestrained *Dnmt3a*$^{R878H/+}$ myeloid cell production. This is consistent with the increased risk of inflammation reported as a severe side effect of pan-TNF inhibitor treatment (28). Here, we have found that targeting TNFR1 versus TNFR2 can separate molecular programs dictating HSC fitness from myeloid cell production such that targeting TNFR1 specifically reduces *Dnmt3a*-mutant HSC fitness while maintaining lineage-balanced output (Fig. 4G). Furthermore, targeting TNFR1 in wild-type HSCs was not observed to have detrimental consequences on hematopoietic output over serial transplantation, supporting that TNFR1 is a unique therapeutic vulnerability of *Dnmt3a*-mutant clones. Given that we identified subsets of *Dnmt3a*-mutant HSCs expressing one or both TNF receptors, further study is needed to determine the extent to which these represent functionally distinct HSC populations.

Reported potential beneficial aspects of *DNMT3A*-mutant clonal hematopoiesis thus far have been related to lymphoid cell production including increased antitumor T cells (7) and maintenance of T-cell immunity during aging (5). Here, we find that TNFα-driven lymphoid cell production from *Dnmt3a*-mutant cells is mediated through TNFR2. Targeting TNFR1 may additionally provide the benefit of boosting adaptive immune function through TNF–TNFR2 signaling, as a lack of TNFR1-mediated TNFα clearance can lead to increased ligand availability for TNFR2 (27). Our work suggests that TNFR1 blockade strategies, such as humanized antibodies that have been shown to have efficacy in inflammatory disease models (28), may be useful in individuals with clonal hematopoiesis who are at high risk of progression to myeloid malignancy. Together, our work suggests that independently manipulating clone fitness and lineage output is possible, which broadens the scope and potential of therapeutic strategies to modulate favorable and unfavorable clonal hematopoiesis outcomes.

METHODS

Experimental Animals

C57BL/6J [The Jackson Laboratory (JAX) stock #00664, RRID:IMSR_JAX:000664, referred to as CD45.2$^+$] and B6.SJL-Ptprca Pepcb/BoyJ (JAX stock #002014, RRID:IMSR_JAX:002014, referred to as CD45.1$^+$) mice were obtained from, and aged within, JAX. *Dnmt3a*$^{fl\text{-}R878H/+}$ mice (JAX stock #032289, RRID: IMSR_JAX:032289) were crossed to B6.CgTg(Mx1-cre)1Cgn/J mice (JAX stock #003556, RRID:IMSR_JAX:003556, referred to as Mx-Cre) or C57BL/6N-*Fgd5*$^{tm3(cre/ERT2)Djr}$/J mice (JAX stock #027789, RRID:IMSR_JAX:027789, referred to as Fgd5-Cre). B6.129S-*Tnfrsf1b*$^{tm1/mx}$; *Tnfrsf1a*$^{tm1/mx}$ mice (JAX stock #003243, RRID:IMSR_JAX:003243) were crossed to *Dnmt3a*$^{fl\text{-}R878H/+}$; Mx-Cre mice. BM from germline *Dnmt3a*$^{+/-}$ and control wild-type mice were provided by G.A. Challen. The Jackson Laboratory's Institutional Animal Care and Use Committee approved all experiments. All genotypes of mice carrying the Mx-Cre allele were given poly(I:C) every other day for a total of five doses between 2 and 4 months of age prior to transplant except where noted below.

Flow Cytometry and Cell Sorting

Single-cell suspensions of BM were prepared by filtering crushed, pooled femurs, tibiae, and iliac crests from each mouse. BM mononuclear cells were isolated by Ficoll-Paque (GE Healthcare Life Sciences) density centrifugation and stained with a combination of fluorochrome-conjugated antibodies from eBioscience, BD Biosciences, or BioLegend—CD45.1 (clone A20), CD45.2 (clone 104), c-Kit (clone 2B8), Sca-1 (clone 108129), CD150 (clone TC15-12F12.2), CD48 (clone HM48-1), FLT3 (clone A2F10), CD34 (clone RAM34), FcgR (clone 2.4G2)—mature lineage (Lin) marker mix, and a viability stain. Stained cells were sorted using a FACSAria II (RRID:SCR_018091) or a FACSymphony S6 Sorter (BD Biosciences), or analyzed on a FACSymphony A5 or LSR II (RRID:SCR_002159) with Diva software (BD Biosciences, RRID:SCR_001456). Surface marker profiles are listed in Supplementary Methods. PB samples were stained and analyzed using a cocktail of CD45.1, CD45.2, CD11b (clone M1/70), B220 (clone RA3-6B2), CD3e (clone 145-2C11), Ly6g (clone 1A8), and Ly6c (clone HK1.4) on an LSR II (BD Biosciences). Gating analysis was performed using FlowJo software v10 (RRID:SCR_008520).

Transplants into Young and Aged Recipient Mice

Two months after poly(I:C), 2×10^6 post-ficoll whole BM cells from *Dnmt3a*$^{+/+}$ Mx-Cre or *Dnmt3a*$^{fl\text{-}R878H/+}$ Mx-Cre donors were transplanted into lethally irradiated (10 Gy), young (2–4 months) or middle-aged (13–15 months) CD45.1$^+$ recipient mice. All transplant recipient mice were monitored every 4 weeks after transplant by flow cytometry analysis of PB and were harvested for BM analysis at 40 weeks after transplant.

Polyvinyl Alcohol Culture and Transplants

Two months after poly(I:C), 25 CD45.2$^+$ HSCs from *Dnmt3a*$^{+/+}$ Mx-Cre or *Dnmt3a*$^{fl\text{-}R878H/+}$ Mx-Cre donors (CD45.2$^+$) and 25 CD45.1$^+$/CD45.2$^+$ HSCs were sorted into a 96-well plate with Ham's F12 media containing final concentrations of 1× penicillin–streptomycin–glutamine (Gibco; cat. #10378-016), 10 mmol/L HEPES (Gibco; cat. #15630080), 1× insulin–transferrin–selenium–ethanolamine (Gibco; cat. #51500-056), 100 ng/mL recombinant murine TPO (BioLegend; cat. #593302), 10 ng/mL recombinant murine SCF (STEMCELL Technologies; cat. #78064), and 1 mg/mL polyvinyl alcohol (Sigma; cat. #P8136; ref. 19) ± 10 ng/mL recombinant murine TNFα (PeproTech; cat. #315-01A) and cultured for 7 days at 37°C and 5% CO_2. TNFα was spiked into the cultures on days 4 and 6. On day 7, half of the wells were stained and analyzed by flow cytometry and half of the wells were harvested, mixed with 1×10^6 CD45.1$^+$ post-ficoll whole BM cells, and transplanted into young, lethally irradiated CD45.1$^+$ recipients. PB was tracked monthly for 6 months after transplant via flow cytometry.

Etanercept Transplants

BM cells (1×10^6) from 2- to 4-month-old *Dnmt3a*$^{+/+}$ Mx-Cre or *Dnmt3a*$^{fl\text{-}R878H/+}$ Mx-Cre donors were competitively transplanted with wild-type CD45.1$^+$ CD45.2$^+$ F1 BM cells in 2- to 4-month-old CD45.1$^+$ lethally irradiated recipients. Recipients were allowed to recover for 1 month and then poly(I:C) was administered every other day for a total of five injections to induce Cre expression. Twenty-eight weeks after poly(I:C), BM was harvested, and 5×10^6 whole BM cells were transplanted into 2- to 4-month-old, lethally irradiated CD45.1$^+$ recipients. Twenty-four weeks after secondary transplant, etanercept (25 mg/kg, Millipore Sigma; #Y0001969) or PBS was administered intraperitoneally twice per week for 4 weeks. PB was monitored weekly, and at 28 weeks after transplant, BM was harvested for analysis.

TNFR Knockout Transplants

CD45.2$^+$ cells (1×10^6) were competed against 1×10^6 CD45.1$^+$ whole BM cells and transplanted into aged, lethally irradiated CD45.1$^+$ recipient animals. One month after transplant, recipients received one intraperitoneal injection of poly(I:C) and recombination was checked via PCR on PB. One month after poly(I:C), animals were bled monthly for 16 weeks. BM was harvested, and 4×10^6 whole BM cells were used for secondary transplantation into aged, lethally irradiated recipients. PB was analyzed starting 1 month after transplant and continued monthly for 20 weeks. BM was harvested and analyzed by flow cytometry and Lin$^-$ c-Kit$^+$ CD45.2$^+$ cells were sorted by FACS for single-cell RNA-seq. Complete blood counts were performed on an Advia 120 Hematology Analyzer (Siemens).

Bulk RNA-seq and Analysis

One-month after poly(I:C), 1×10^6 whole BM cells from *Dnmt3a*$^{+/+}$ Mx-Cre or *Dnmt3a*$^{R878H/+}$ Mx-Cre donors were transplanted into sublethally irradiated (6 Gy), young (2 months) or middle-aged (13–15 months) CD45.1$^+$ recipient mice. Recipients were harvested 4 months after transplant for PB and BM analysis. CD45.2$^+$ HSCs were sorted directly into RLT buffer (Qiagen) and flash frozen. Total RNA was isolated using the RNeasy Micro Kit (Qiagen) including DNase treatment, and sample quality was assessed using a NanoDrop 2000 spectrophotometer (Thermo Scientific, RRID:SCR_018042) and RNA 6000 Pico LabChip assay (Agilent Technologies). Libraries were prepared using the Ovation RNA-Seq System V2 (NuGen) and Hyper Prep Kit (Kapa Biosystems). Library quality and concentration were evaluated using the D5000 ScreenTape assay (Agilent) and quantitative PCR (Kapa Biosystems). Libraries were pooled and sequenced 75-bp single end

on the NextSeq (Illumina, RRID:SCR_014983) using NextSeq High Output Kit v2 reagents at a sequencing depth of >30 million reads per sample. Trimmed alignment files were processed using RSEM (v1.2.12, RRID:SCR_013027). Alignment was completed using Bowtie 2 (v2.2.0, RRID:SCR_005476). Expected read counts per gene produced by RSEM were rounded to integer values, filtered to include only genes that had at least two samples within a sample group having a counts per million reads >1, and passed to edgeR (v3.14.0, RRID:SCR_012802) for differential expression analysis. The generalized linear model likelihood ratio test was used for differential expression in pairwise comparisons between sample groups that produced exact *P* values per test. The Benjamini and Hochberg's algorithm (*P* value adjustment) was used to control the false discovery rate (FDR). Features with FDR-adjusted $P < 0.05$ were declared significantly differentially expressed. Differentially expressed genes were investigated for overlap with published datasets using Gene Set Enrichment Analysis (RRID:SCR_003199), and upstream regulators were predicted using Ingenuity Pathway Analysis software (Qiagen, RRID:SCR_008653).

Single-Cell RNA-seq and Analysis

Cells were counted on a Countess II automated cell counter (Thermo Fisher), and 12,000 cells were loaded onto one lane of a 10X Chromium microfluidic chip (10X Genomics). Single-cell capture, barcoding, and library preparation were performed using the 10X Chromium version 3.1 chemistry according to the manufacturer's protocol (#CG000315). cDNA and libraries were checked for quality on Agilent 4200 Tapestation (RRID:SCR_019398) and quantified by KAPA qPCR before sequencing; each gene-expression library was sequenced at 18.75% of an Illumina NovaSeq 6000 (RRID:SCR_016387) S4 flow cell lane, targeting 6,000 barcoded cells with an average sequencing depth of 75,000 reads per cell. Illumina base call files for all libraries were demultiplexed and converted to FASTQs using bcl2fastq v2.20.0.422 (Illumina, RRID:SCR_015058). The Cell Ranger pipeline (10X Genomics, version 6.0.0, RRID:SCR_017344) was used to align reads to the mouse reference GRCm38.p93 (mm10 10X Genomics reference 2020-A), deduplicate reads, call cells, and generate cell by gene digital count matrices for each library. The resultant count matrices were uploaded into PartekFlow (version 10.0.22.0428) for downstream analysis and visualization. This included log transformation of count data, principal component analysis, graph-based clustering from the top 20 principal components using the Louvain algorithm, Uniform Manifold Approximation and Projection (UMAP) visualization, and pathway enrichment analysis. Trajectory and pseudotime analyses were performed using Monocle 3 (RRID:SCR_018685).

Statistical Analysis

No sample group randomization or blinding was performed. All statistical tests, including evaluation of the normal distribution of data and examination of variance between groups being statistically compared, were assessed using Prism 9 software (GraphPad, RRID:SCR_002798).

Data Availability Statement

All data in this study are deposited in the NCBI Gene Expression Omnibus (RRID:SCR_005012) under accession numbers GSE189406 (bulk RNA-seq) and GSE203550 (single-cell RNA-seq).

Authors' Disclosures

J.M. SanMiguel reports grants from the NIH and from the American Society of Hematology during the conduct of the study, as well as a patent for D21-017-USPROV1 pending. L.S. Schwartz reports grants—Burroughs Wellcome Training Fellow and Ruth L. Kirschstein Predoctoral Individual National Research Service Award—outside the submitted work. J.J. Trowbridge reports grants from the NIH, the EvansMDS Foundation, the Leukemia & Lymphoma Society, the American Society of Hematology, the Ellison Medical Foundation, V the Foundation, and the Maine Cancer Foundation during the conduct of the study; other support from H3 Biomedicine outside the submitted work; and a patent for D21-017-USPROV1 pending and a patent for US20130209430A1 issued, licensed, and with royalties paid from Fate Therapeutics. No disclosures were reported by the other authors.

Authors' Contributions

J.M. SanMiguel: Conceptualization, data curation, formal analysis, validation, investigation, visualization, methodology, writing–original draft. **E. Eudy:** Investigation, visualization, writing–review and editing. **M.A. Loberg:** Investigation, visualization, writing–review and editing. **K.A. Young:** Formal analysis, investigation, writing–review and editing. **J.J. Mistry:** Formal analysis, investigation, writing–review and editing. **K.D. Mujica:** Validation, investigation, methodology, writing–review and editing. **L.S. Schwartz:** Formal analysis, investigation, writing–review and editing. **T.M. Stearns:** Data curation, formal analysis, writing–review and editing. **G.A. Challen:** Resources, writing–review and editing. **J.J. Trowbridge:** Conceptualization, supervision, funding acquisition, visualization, writing–original draft.

Acknowledgments

We thank all members of the Trowbridge lab for their help with experimental support and manuscript editing and Scientific Services at The Jackson Laboratory. We thank Ross Levine, Coleman Lindsley, and Michael Rauh for discussions and input, and Dan Landau and Neville Dusaj for providing single-cell expression data from human *DNMT3A*-mutant clonal hematopoiesis samples. This work was supported by NIH U01AG077925 (J.J. Trowbridge), NIH R01DK118072 (J.J. Trowbridge), NIH R01AG069010 (J.J. Trowbridge), and an Evans-MDS Discovery Research Grant (J.J. Trowbridge). This study was supported in part by The Jackson Laboratory's Cancer Center Support Grant NIH P30CA034196. L.S. Schwartz was supported by NIH F31DK127573. J.M. SanMiguel was supported by NIH T32AG062409, NIH T32HD007065, and an American Society of Hematology Scholar Award. J.J. Mistry was supported by a JAX Scholar award. G.A. Challen and J.J. Trowbridge are scholars of the Leukemia & Lymphoma Society. G.A. Challen was supported by NIH R01DK124883.

Note

Supplementary data for this article are available at Cancer Discovery Online (http://cancerdiscovery.aacrjournals.org/).

Received January 21, 2022; revised July 11, 2022; accepted September 15, 2022; published first September 28, 2022.

REFERENCES

1. Kim PG, Niroula A, Shkolnik V, McConkey M, Lin AE, Słabicki M, et al. Dnmt3a-mutated clonal hematopoiesis promotes osteoporosis. J Exp Med 2021;218:e20211872.
2. Genovese G, Kähler AK, Handsaker RE, Lindberg J, Rose SA, Bakhoum SF, et al. Clonal hematopoiesis and blood-cancer risk inferred from blood DNA sequence. N Engl J Med 2014;371:2477–87.
3. Jaiswal S, Fontanillas P, Flannick J, Manning A, Grauman PV, Mar BG, et al. Age-related clonal hematopoiesis associated with adverse outcomes. N Engl J Med 2014;371:2488–98.
4. Trowbridge JJ, Starczynowski DT. Innate immune pathways and inflammation in hematopoietic aging, clonal hematopoiesis, and MDS. J Exp Med 2021;218:1–15.
5. van den Akker EB, Pitts SJ, Deelen J, Moed MH, Potluri S, van Rooij J, et al. Uncompromised 10-year survival of oldest old carrying somatic mutations in DNMT3A and TET2. Blood 2016;127:1512–5.
6. Bouzid H, Belk J, Jan M, Qi Y, Sarnowski C, Wirth S, et al. Clonal hematopoiesis is associated with reduced risk of Alzheimer's disease. Blood 2021;138:5.

7. Gibson CJ, Kim HT, Zhao L, Murdock HM, Hambley B, Ogata A, et al. Donor clonal hematopoiesis and recipient outcomes after transplantation. J Clin Oncol 2022;40:189–201.
8. van den Akker EB, Makrodimitris S, Hulsman M, Brugman MH, Nikolic T, Bradley T, et al. Dynamic clonal hematopoiesis and functional T-cell immunity in a supercentenarian. Leukemia 2021;35:2125–9.
9. Loberg MA, Bell RK, Goodwin LO, Eudy E, Miles LA, SanMiguel JM, et al. Sequentially inducible mouse models reveal that Npm1 mutation causes malignant transformation of Dnmt3a-mutant clonal hematopoiesis. Leukemia 2019;33:1635–49.
10. Young K, Eudy E, Bell R, Loberg MA, Stearns T, Sharma D, et al. Decline in IGF1 in the bone marrow microenvironment initiates hematopoietic stem cell aging. Cell Stem Cell 2021;28:1473–82.
11. Linton PJ, Dorshkind K. Age-related changes in lymphocyte development and function. Nat Immunol 2004;5:133–9.
12. Cao X, Wu X, Frassica D, Yu B, Pang L, Xian L, et al. Irradiation induces bone injury by damaging bone marrow microenvironment for stem cells. Proc Natl Acad Sci U S A 2011;108:1609–14.
13. Li J, Kwong DLW, Chan GCF. The effects of various irradiation doses on the growth and differentiation of marrow-derived human mesenchymal stromal cells. Pediatr Transplant 2007;11:379–87.
14. Cook EK, Izukawa T, Young S, Rosen G, Jamali M, Zhang L, et al. Comorbid and inflammatory characteristics of genetic subtypes of clonal hematopoiesis. Blood Adv 2019;3:2482–6.
15. Yamashita M, Passegué E. TNF-α coordinates hematopoietic stem cell survival and myeloid regeneration. Cell Stem Cell 2019;25:357–72.e7.
16. Ivanova NB, Dimos JT, Schaniel C, Hackney JA, Moore KA, Lemischka IR. A stem cell molecular signature. Science 2002;298:601–4.
17. Eppert K, Takenaka K, Lechman ER, Waldron L, Nilsson B, van Galen P, et al. Stem cell gene expression programs influence clinical outcome in human leukemia. Nat Med 2011;17:1086–93.
18. Nam AS, Dusaj N, Izzo F, Murali R, Myers RM, Mouhieddine T, et al. Single-cell multi-omics of human clonal hematopoiesis reveals that DNMT3A R882 mutations perturb early progenitor states through selective hypomethylation. Nat Genet 2022;54:1514–26.
19. Wilkinson AC, Ishida R, Kikuchi M, Sudo K, Morita M, Crisostomo RV, et al. Long-term ex vivo haematopoietic-stem-cell expansion allows nonconditioned transplantation. Nature 2019;571:117–21.
20. Giladi A, Paul F, Herzog Y, Lubling Y, Weiner A, Yofe I, et al. Single-cell characterization of haematopoietic progenitors and their trajectories in homeostasis and perturbed haematopoiesis. Nat Cell Biol 2018;20:836–46.
21. Jeong M, Park HJ, Celik H, Ostrander EL, Reyes JM, Guzman A, et al. Loss of Dnmt3a immortalizes hematopoietic stem cells in vivo. Cell Rep 2018;23:1–10.
22. Cai Z, Kotzin JJ, Ramdas B, Chen S, Nelanuthala S, Palam LR, et al. Inhibition of inflammatory signaling in Tet2 mutant preleukemic cells mitigates stress-induced abnormalities and clonal hematopoiesis. Cell Stem Cell 2018;23:833–49.
23. Fuster JJ, Zuriaga MA, Zorita V, MacLauchlan S, Polackal MN, Viana-Huete V, et al. TET2-loss-of-function-driven clonal hematopoiesis exacerbates experimental insulin resistance in aging and obesity. Cell Rep 2020;33:108326.
24. Meisel M, Hinterleitner R, Pacis A, Chen L, Earley ZM, Mayassi T, et al. Microbial signals drive pre-leukaemic myeloproliferation in a Tet2-deficient host. Nature 2018;557:580–4.
25. Abegunde SO, Buckstein R, Wells RA, Rauh MJ. An inflammatory environment containing TNFα favors Tet2-mutant clonal hematopoiesis. Exp Hematol 2018;59:60–5.
26. Cook EK, Luo M, Rauh MJ. Clonal hematopoiesis and inflammation: partners in leukemogenesis and comorbidity. Exp Hematol 2020;83:85–94.
27. Fischer R, Kontermann R, Maier O. Targeting sTNF/TNFR1 signaling as a new therapeutic strategy. Antibodies 2015;4:48–70.
28. Richter F, Williams SK, John K, Huber C, Vaslin C, Zanker H, et al. The TNFR1 antagonist atrosimab is therapeutic in mouse models of acute and chronic inflammation. Front Immunol 2021;12:1–14.